Machine learning-driven energy management of a hybrid nuclear-wind-solar-desalination plant

Vazquez Pombo, Daniel; Bindner, Henrik W.; Spataru, Sergiu Viorel; Sørensen, Poul Ejnar; Rygaard, Martin

Published in:
Desalination

Link to article, DOI:
10.1016/j.desal.2022.115871

Publication date:
2022

Document Version
Publisher's PDF, also known as Version of record

Desalination 537 (2022) 115871

Contents lists available at ScienceDirect

Desalination

journal homepage: www.elsevier.com/locate/desal

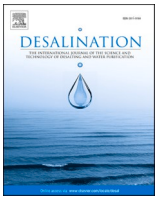

Machine learning-driven energy management of a hybrid nuclear-wind-solar-desalination plant

Daniel Vázquez Pombo [a,b,*], Henrik W. Bindner [a], Sergiu V. Spataru [c], Poul E. Sørensen [a], Martin Rygaard [d]

[a] Wind and Energy Systems, Technical University of Denmark (DTU), Frederikborsvej 399, Roskilde 4000, Denmark
[b] R&D Strategic Development, Vattenfall AB, Evenemangsgatan 13C, Solna 169 56, Sweden
[c] Department of Photonics Engineering, Technical University of Denmark, Frederikborsvej 399, Roskilde 4000, Denmark
[d] Department of Environmental Engineering, Water Technology and Processes, Technical University of Denmark, Lyngby 2800, Denmark

HIGHLIGHTS

- A hybrid power plant concept aiming simultaneous decarbonization of electricity and water sectors is proposed.
- An energy management system integrating physics informed machine learning forecasts is presented.
- Synergies between electrical, water and heat sectors are exploited, improving renewable integration.
- The stochastic dispatcher is suitable for real time implementation and presents a robust performance.

ARTICLE INFO

Keywords:
SMR
Stochastic dispatch
Desalination
Hybrid power plant
Machine learning

ABSTRACT

The ongoing energy transition and incoming water scarcity crisis demand coordinated research to ensure a fossil-free future for humankind. Aiming to increase energy efficiency, reduce curtailment and decarbonize water production, this paper proposes a novel energy management system (EMS) for a hybrid plant compound by a small modular nuclear reactor acting as cogeneration unit, a wind and solar farms as generators. Additionally reverse osmosis and multi-stage flash desalination plants are included as demand responsive units along with a freshwater storage. Mixed integer linear programming (MILP) is employed to formulate this stochastic optimization problem, where piecewise linear functions define operational costs and efficiencies of SMR and desalination motivating energy efficiency and safety. Renewable availability point forecasts are obtained with physics informed machine learning models whose error is characterised by fitting the predictor's residuals to different statistical distributions following an unsupervised methodology. The suitability of the EMS is addressed in two study cases, one exploring the flexibility exploitation of the algorithm and another proving its suitability for real-time implementation. The dispatcher manages to keep unaltered the SMR's core reaction while satisfying both electrical and water demand in different renewable availability regimes by fully exploiting sector coupling flexibility. Simultaneously, renewable curtailment is kept to a minimum.

1. Introduction

Water scarcity crisis is expected to directly affect 40% of human population by 2030 [1]. Despite alternatives such as groundwater utilization, reclaimed wastewater, or rain harvesting; desalination is an inevitable solution in many areas such as Australia, US, Spain, Africa, and the Middle East [2]. Disregarding the specific approach, desalination is an energy intensive process whose current and future demand pose additional strain in the energy sector, thus representing significant greenhouse emissions [3].

A number of scientific contributions proposed methods to reduce the energy impact and emissions of desalination. Some focus directly on the energy efficiency of the desalination process such as Tian et al. [4], who explore the usage of microwave radiation in flash evaporation processes, reaching nearly 80% efficiency. Zhang et al. [5] performed an analysis on osmotically-assisted reverse osmosis and batch-operated vacuum-air-gap distillation concluding on its good economic performance

* Corresponding author at: Wind and Energy Systems, Technical University of Denmark (DTU), Frederikborsvej 399, Roskilde 4000, Denmark.
E-mail address: dvapo@elektro.dtu.dk (D.V. Pombo).

https://doi.org/10.1016/j.desal.2022.115871
Received 25 February 2022; Received in revised form 14 May 2022; Accepted 19 May 2022
Available online 9 June 2022

Nomenclature

Sets and Indices

0	Initial
a, b, c, d, f	Operation, on, off, ramping, and deviation
$\mathscr{D}$	Demand response technologies
$\mathscr{O} \subseteq \mathscr{D}$	Reverse osmosis desalination plants
$\mathscr{E} \subseteq \mathscr{D}$	Multi-stage flash desalination plants
$\mathscr{G}$	Generators
$\mathscr{G}^R \subseteq \mathscr{G}$	Renewable source generators
$\mathscr{G}^N \subseteq \mathscr{G}$	SMR units generators
e, h, n, w	Electricity, heat, nuclear, and water
U/D	Up/down
$y \in Y$	Non-linear value y of function Y
$l \in L$	Segment of the piecewise linear function
$t \in T$	Time periods
$\varnothing \in \Phi$	Scenarios
Ξ	Set of all variables

Parameters

A_j^y	Piecewise linear coefficient
$\overline{D_j^R}$	Maximum ramp-down limit [MW]
$\overline{D_j^S}$	Maximum power before shut-down [MW]
$\overline{E}^T, E^T$	Maximum/minimum freshwater requirements
$\mathscr{F}_{t,\,\phi,\,r}$	Forecasted renewable available power
$\overline{H}_{n/d}$	Maximum heat power limit [MW]
$\mathscr{L}_t^{e/w}$	Electric/water demand [MW] or [m^3]
$\widetilde{P_{t,r}}$	Renewable power availability [MW]
$\overline{P}_j, Pj$	Maximum/minimum power limit [MW]
$\overline{PCC}$	Point of common coupling capacity [MW]
T_j^{down}	Minimum off time [periods t]
T_j^{off}	Number of periods t until decommission
$\overline{T_j^{up}}, T_j^{up}$	Maximum/minimum on time [periods t]
$\overline{T0_j^{up}}, \overline{T0_j^{down}}$	Maximum on/off time from initial t
$T0_j^{up}, T0_j^{down}$	Minimum on/off time from initial t
$\overline{U_j^S}$	Maximum start-up power [MW]
$\overline{U_j^R}$	Maximum ramp-up limit [MW]
$\overline{W^{ds}}$	Water storage discharge limit [m^3/h]
$\overline{W}^S, W^S$	Maximum, minimum state of charge
α, β, θ	Quadratic function coefficients
γ_ε	Heat to electricity conversion factor [%]
$\sigma_t^{e/w}$	Selling prize [â,¬/MWh] or [â,¬/m^3]
χ_ϕ	Probability of scenario ϕ [%]

Variables

$\mathscr{C}_t^a$	Operational cost of time t [€/MWh]
$\mathscr{C}_t^b$	Start-up cost of time t [€/MWh]
$\mathscr{C}_t^c$	Shut-down cost of time t [€/MWh]
$\mathscr{C}_t^d$	Reactor ramping cost of time t [€/MWh]
$\mathscr{C}_t^f$	Reactor derating cost of time t [€/MWh]
$\mathscr{I}_t^e$	Electricity market income [€/MWh]
$\mathscr{I}_t^w$	Freshwater market income [€/MWh]
$P_{t,\,\phi,\,j}^c$	Curtailed renewable power [MW]
$P_{t,\,j}^e$	Scheduled DA electric power [MW]
$P_{t,\,n}^N$	Scheduled DA reactor power [MW]
$P_{t,\,n/w}^H$	Scheduled DA heat power [MW]
$Q_{t,\,j}$	Max available electric power [MW]
$R_{t,\,j}^D$	Scheduled DA downward reserve [MW]
$r_{t,\,\phi,\,j}^D$	RT downward reserve [MW]
$R_{t,\,j}^U$	Scheduled DA upward reserve [MW]
$r_{t,\,\phi,\,j}^U$	RT upward reserve [MW]
$W_t^{ch/ds}$	Charged/discharged water from storage [m^3]
$W_t^{\mathscr{S}}$	Water storage state of charge [m^3]
$\delta_{t,\,j}^{l,\,x}$	Value from x piecewise linear parameter
$\eta_{t,\,j}$	Electricity to water conversion factor [%]
$\nu_{t,\,j}$	Binary. 1 if online, and 0 otherwise
$\rho_{t,\,j}$	Cost [€/MWh]

particularly when using renewable energy. On the other hand, others focus on coupling renewable energy source (RES) with different desalination technologies. For instance, Moharram et al. [6]; employed a solar powered Rankine cycle operating at full efficiency using excess heat to run a desalination stage. Others like Mo et al. [7] studied the influence of variable energy prices in the cost of freshwater and the possibilities for demand response. More recently, Mito et al. [8] proposed using model predictive control to integrate reverse osmosis (RO) with renewable energy. However, there has been a shift towards hybrid power plants (HyPP) given their higher efficiency, increased functionalities, and dispatchability [9]. In this direction, Sadeghi et al. [10] performed an economic assessment of desalinated water for scenarios in which energy is obtained from solar, small modular reactor (SMR) or both; concluding on the superiority of the HyPP structure. While Liu et al. [11] integrate freshwater storage, wind and solar power in a coastal desalination installation to reduce the water production costs.

Despite their advantages, HyPP present challenges regarding asset coordination, which has motivated extensive research in energy management systems (EMS). For instance, the dispatchability of a wind and concentrated solar HyPP is discussed in [12] including operational risk in the EMS. While Yang et al. [13] use stochastic unit commitment (SUC) to deal with extreme weather at system level. Furthermore, Le et al. [14] highlight the capability of SUC of enabling load-shifting in the day-ahead (DA) stage and reserve-capacity in the real-time (RT). While Van der Meer, et al. [15] coordinate solar PV, batteries and uncontrollable load in a prosumer building using SUC. However, SUC limitations are the forecast need, scenario definition and characterisation, which caused authors like Amabile et al. [16] to use rule-based dispatchers to coordinate a smart building with solar, storage and demand responsive (DR) units. Nevertheless, off-the-shelf forecasters based on machine learning (ML) wide availability and their documented suitability for wind and solar prediction [17] justifies the need for methods translating point forecasts into stochastic scenarios [18]. Yet, uncertainty characterisation and validation is far from trivial [19]. Existing methods combine point and uncertainty forecasts into hybrid models [20], whose main disadvantage is requiring two separate models.

This work aims to contribute the scientific community by proposing an EMS for a HyPP compound by an SMR, a PV plant, a wind farm (WF), and two different desalination technologies; one requiring only electrical input, and the other demanding also thermal. The objective is to enable carbon-free electricity and freshwater production for any given region, as the HyPP could also operate as an isolated system. The dispatcher is formulated as an optimal SUC where the uncertainty is assumed caused by the wind and solar resource. The available RES power is estimated using physics informed ML to train of-the-shelf point forecasters. Then, stochastic scenarios are characterised based on the probability distribution of the forecast residuals, by fitting them to a known statistical distribution with an unsupervised approach. The suitability of the proposed HyPP, EMS, forecast, and uncertainty

modeling is evaluated in different study cases studying the influence of RES availability, forecast accuracy and scenario characterisation.

The paper is structured as follows: Section 2 presents the HyPP concept object of study, Section 3 presents the formulation of the EMS, Section 3.2 introduces the employed physics informed ML applied to wind and solar forecasting and the scenario generation process. Then, Section 4 presents the study cases, and Section 5 concludes the paper.

2. Background

The considered nuclear reactor and desalination technologies are integrated into the HyPP concept in this section.

2.1. Small Modular Reactors

The main features characterising SMR are: to have an output power lower than 300 MWe, to have a design allowing them to be manufactured, and fueled at a factory and, then, be delivered to their definitive site. Furthermore, they offer enhanced security, safety and are, by design, able to offer de-rated operation and load-following capabilities. [21]

Load following mode allows to continuously modify the reactor output power in order to follow electric demand. This is achieved by controlling the reactor's reactivity by modifying the position of the control rods in the core [22]. This operational mode contributes to poisoning traditional reactors, due to the apparition of undesired fission products that act as parasitic neutron absorbers, introducing negative reactivity. Those products accumulate in the reactor over time eventually preventing achieving supercriticality. SMR design and fuel selection minimizes the apparition of such products, however, de-rated operation results still economically inefficient as reducing the output does not significantly affect the fuel consumption rate nor the operating expenses. In addition, they suffer thermo-mechanical stresses derived from frequent rampings. Hence, even if SMR are capable of derated operation, it is desirable to avoid it [23].

There are two alternatives to de-rating the core in order to perform load following. One is to couple it with a dump load, or demand responsive unit that will allow to effectively derate the electric output without affecting the SMR's operation. Another alternative is to bypass some of the steam from the turbine into a heat sink. In that sense, cogeneration of hydrogen, desalination and district heating have been deemed suitable in different studies [24,25].

There are a few SMR designs available such as CAREM-25, CANDU, and NuScale. However, the latter presents higher technology readiness level as it received design approval in 2021 and targets first commercial operation in 2027 [21]. NuScale, focus of this study, is a small, light-water pressurized-water reactor with natural circulation employing UO_2 pellets with $>4.95\%$ U^{235} enrichment. NuScale design power is 160 MWt and 45 MWe, is scalable up to 12 modules in a single facility, and is suitable for cogeneration [26].

2.2. Desalination technologies

The most important desalination processes at commercial stage can be divided into distillation and membrane based. The first require mainly thermal energy to be complemented with electricity while the second only employs electricity. Rather than an exhaustive review, this section presents the most important technology of each category.

Reverse Osmosis is a process in which a semi-permeable membrane separates desalinated water from a saline concentrate stream. The applied pressure must overcome the osmotic as determined by the feed water salinity. It usually includes two compression stages, requiring in total about 2–5 kWh/m^3 of electricity. Furthermore, inlet water requires pretreatment to maintain production capacity over time. As the most efficient and flexible desalination method (whose rampings are disregarded in hour scale), RO represents 50% of the global capacity. [27]

Multi-Stage Flash Distillation (MSF) is the most representative distillation technology by global installed capacity. A typical setup consists of two sections, brine heater and flashing stages. The in-feed is preheated in a series of heat exchangers prior to entering a brine heater for further heating and pressure increase. The hot and pressurized water passes into a flash stage where pressure is lower causing a fast vaporization followed by condensation on a heat exchanger. There, the heat is recovered by new in-feed water and the distillate is collected. The remaining saline water continues repeating this process in up to 25 successive flashing stages, until it is discharged back to the inlet source. Net energy wise, MSF requires 2.5–5 kWh/m^3 of electric input to operate pumps and other devices, and 15.8–23.5 kWh/m^3 of heat [28]. To increase efficiency and due to their thermal requirements, MSF are usually integrated in co-generation systems. There, exergy-rich steam is turbined for electricity generation, while its counterpart is employed in the MSF [29]. In such systems, the thermal generator is the most constrained in terms of ramping, startup and shutdown dynamics, thus dismissing those of the MSF. However, based on the studies from Al-Fulaij et al. [30], we can establish a conservative estimation of 60%/h ramping, a minimum running of 30% and a minimum on period of 4 hours.

The main advantages of RO are lower energy needs, faster ramping, and modularity, while being more prone to failures. MSF presents slower dynamics due to thermal inertias, but is more robust, less affected by infed variations, and produces higher quality freshwater. In [31] RO and MSF are studied as combined units by feeding seawater to each process separately and mixing the output. Besides reducing costs related to construction, pre-, and post-treatment, the RO process is simplified increasing reliability. [6,32]

2.3. Hybrid power plant

The aggregation of different generation technologies is a topic gaining increasing interests, particularly in the context of RES integration. The main objective is to coordinate dispatch, reduce construction costs, increase the plant's efficiency, overinstallation at the same point-of-common-coupling (PCC), etc. However, they present other advantages as reducing stochasticity impact of the renewable units [33]. Furthermore, besides generation units, the HyPP concept allows to integrate demand responsive units such as desalination [34]. Fig. 1 depicts a HyPP combining a SMR, a WF and a PV plant as generators, with RO and MSF as DR units. Note how the output steam from the generator can be redirected to the MSF via a heat exchanger. In that way, the desalination system is protected from neutron leaks.

3. Methodology

We propose a coordinated EMS approach formulated as a stochastic MILP maximizing the HyPP profits. The algorithm assumes DA market prices as given and integrates RES-related uncertainty with a number of scenarios. These, are generated based on the output of physics informed ML forecasters and their error characterisation. Fig. 2 presents the EMS architecture and data flow. In general, the inputs to the EMS are commands sent by the system operator, Market signals such as prices, point forecasts and their associated probability. Since we employ a ML-based approach, said forecasts are of course computed based on current and historical measurements. This section gently introduces the optimization problem and the forecasters. However, the interested reader is referred to Annex A for a full description of the mathematical formulation.

3.1. EMS stochastic optimization

In general, the objective function of the EMS aims to maximize profit by minimize the difference between costs and income. Costs are in general related to usage, initialization, start-up, and shutdown, but in particular for the SMR, a term accounting for the additional stressed

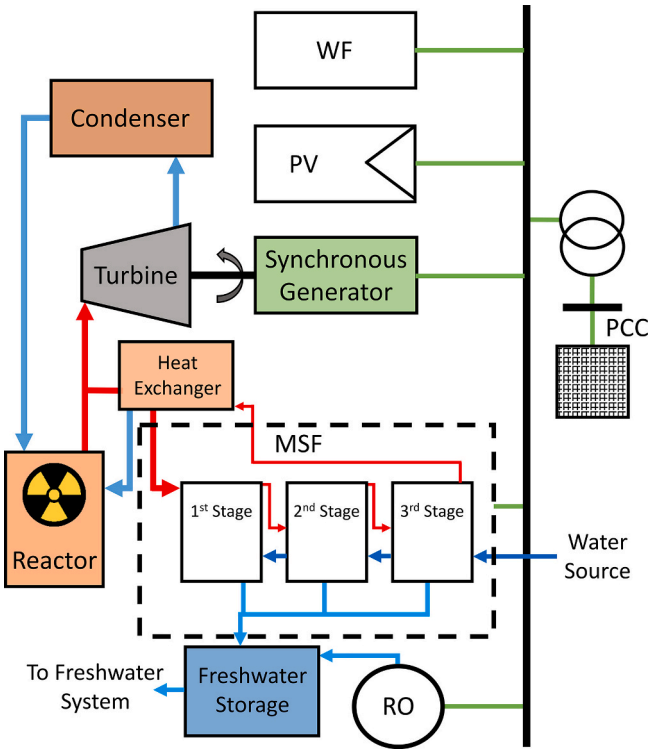

Fig. 1. Considered HyPP layout.

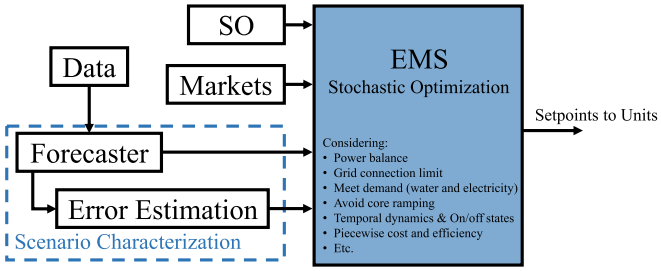

Fig. 2. Concept of a data-driven stochastic EMS.

posed by de-rated operation is included. On the other hand, income is related to selling the scheduled water and electricity production including reserve. Constraints are then related to the operational limits of the connection point and the individual units, such as the minimum and maximum power capabilities, ramping, minimum and maximum on/off periods, etc. In the case of the SMR, additional equations are needed to bound the heat and electrical production with the core's reaction, and with the heat requirements of the MSF. Similarly, the cost function of the SMR and the efficiency curves of desalination plants are accounted for using a piecewise linearization of their typical curves. Furthermore, it is possible to consider the inclusion of a water storage which adds an additional level of flexibility to the system.

3.2. Physics informed forecasting

Physics informed ML is a sub-set of data-driven forecasting methods that can be applied to time series. Its main characteristic is to introduce knowledge of the physical dependencies among the different metrics available in the dataset in the ML model [35]. In this work, data with hourly resolution was used to train two different ML models for predicting wind and PV power. The ML methods were RF and a hybrid CNN-LSTM artificial neural networks as they are two of the best predictors reported in the literature [17]. The employed dataset, SOLETE, includes metrics such as: irradiance, wind speed, humidity, etc. from 1st June 2018 to 1st September 2019 [36].

The, ML models were trained using mean absolute error (MAE) as the optimizer metric (1). While root mean squared error (RMSE) is used in their evaluation (2). All the models were developed in Python using open access libraries such as Scikit-learn and TensorFlow.

$$MAE_h = \frac{\sum_i^n \left| \mathscr{F}_{i,h} - \widehat{\mathscr{F}}_{i,h} \right|}{n}, \quad \forall h \in \mathscr{H} \tag{1}$$

$$RMSE_h = \sqrt{\frac{\sum_i^n \left(\mathscr{F}_{i,h} - \widehat{\mathscr{F}}_{i,h} \right)^2}{n}}, \quad \forall h \in \mathscr{H} \tag{2}$$

where $\mathscr{F}$, $\widehat{\mathscr{F}}$, n, and h stand for observation, prediction, sample number and time step.

3.2.1. Solar

The Solar forecaster was developed according to the physics-informed approach described in [37]. That is, by integrating the King's PV performance [38] in the ML-model. King's model allows estimating the operating temperature, and available power, while requiring basic meteorological metrics and datasheet parameters from the PV panels and the inverter. The resulting RF model was trained using: humidity, irradiance in the plain of array, estimated panel temperature, and hour of the day.

3.2.2. Wind

On the other hand, the turbine's datasheet power curve is avoided to estimate available power as the wind speed measurement point and the turbine are located about 200 m apart. The effective power curve is then obtained by training a RF with wind speed, direction, and power as features. Then, following the recommendations in [39], a second RF and a CNN-LSTM models were trained to predict power. The RF used mean and standard deviation of the previous 24 hours, while CNN-LSTM included humidity in addition. Stacking is a special case of model averaging aiming to improve response time, stability and accuracy of ML models [40]. The wind forecaster is built by stacking the effective power curve of the turbine with either the second RF or the CNN-LSTM model.

3.3. Scenario characterisation

From an stochastic optimization perspective, scenarios are characterised by their occurrence likelihood. However, the proposed point forecasters, the most commonly encountered in scientific literature, return an average or median expected value, not a probability density function (pdf). Yet, fundamental statistics allow to fit recordings to a number of well-established probability distributions. For instance, Hodge et al. [41] used Gaussian, Weibull and Cauchi distributions to study wind power forecast errors; concluding that the effective distribution cannot be assumed. Then, Wu et al. [42] developed a mixed LaPlace-Gaussian distribution to model persistence-based forecasts for wind power. While Yan et al. [43] consider analysing PV power forecasting error distribution using a Gauss model. Note that the common limitation of the aforementioned work is to limit their analysis to few distributions, or to develop complex tailor-made solutions.

In order to generate different scenarios and their respective probabilities, we characterise the error distribution per sample based on the ML-model's performance. First, the residuals are computed for each $t \in T$ of the validation set in p.u. based on the installation size. Then, these are fitted to the 100 different distributions available in SciPy [44] such as: Gaussian, Weibull, Beta, Cauchi, etc. and their pdfs are obtained. Afterwards, the residual sum of squares (RSS), (3), is used to rank the methods, while the coefficient of determination (R^2), (4), is used as tie-breaker. Once the best fit distribution is found for each sample, their pdf can be used to obtain the related residuals at given quantiles. Therefore, when a new forecast is casted, its computed pdf is used to estimate

different scenarios and their probability based on a desired set of quantiles. This methodology is depicted in Fig. 3.

$$RSS = \sum_{i}^{n} |\mathscr{F}_i - \widehat{\mathscr{F}}_i|^2, \tag{3}$$

$$R^2 = \frac{RSS}{\sum_{i}^{n} \left| \mathscr{F}_i - \overline{y}_i \right|}, \tag{4}$$

The fitted distributions per resource, method and sample are presented in Fig. 4. The maximum R^2 was 0.99, the minimum 0.70, and the average 0.89; being homogeneous for wind and solar and both forecasting methods. Left-skewed Levy distribution is the most common but it only appears in CNN-LSTM for wind power, in general Gen Normal and Cauchi are the most repeated across the rest of the predictors. Still, CNN-LSTM presented higher distribution homogeneity, which is consistent with the ANN's capacity of capturing temporal correlations.

By estimating error distribution for each sample independently, temporal correlations within the time-series are diluted. This might lead to defining scenarios presenting higher error sparsity than those naturally occurring. This limitation is however only relevant for systems where energy dispatch is severely constricted, such as those critically dependent on energy storage-based load shifting [45]. Furthermore, several studies point towards the general lack of temporal correlation of short term wind power measurements [46], which allows dismissing them. The advantages of the proposed method are related to the unsupervised fit that avoids preconceptions and guesses related to the residual distribution. In addition, it is suitable for any time-series and thus can be applied to both wind and solar power as well as to other fields.

4. Study case

This section presents two study cases using the HyPP from Fig. 1: A explores the influence of available RES and forecaster accuracy in the EMS; while B explores the effect of including larger number of quantiles in the accuracy and computational performance. Note that the optimization problem has been formulated in Pyomo, and solved using a commercial solver called Gurobi [47].

The considered generation units are a NuScale SMR of 45/160 MWe/MWth, a 20 MW WF, and a 10 MW PV, while the DR units are a 20 MW RO, and a 150/30 MWt/MWe MSF; and a 100 m^3 WS with an initial level of 30%. A summary of implemented parameters is made available to the reader in the Complementary Data section. The operational costs of each technology have been estimated based on a survey of different documents [48–51]. Lastly, the PCC is limited to 50 MW, which can be objectively considered as a small interconnection capacity. This value is selected to highlight the flexibility provided by the proposed EMS. Even though such value is usually related to the substation capacity, in the context of energy islands or isolated regions, it can be used as a dynamic parameter representing the allocation capacity limit of the local grid. In that case, the PCC limitation can be used to maximize grid usage

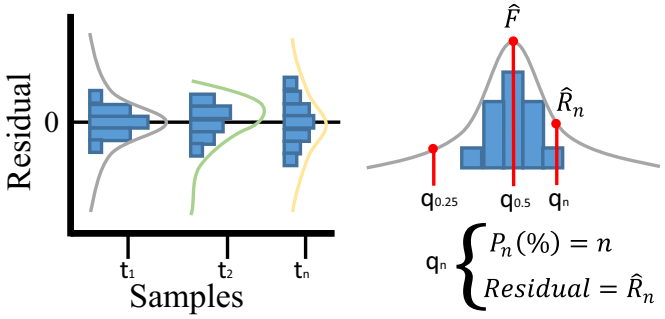

Fig. 3. Residual distribution characterisation concept.

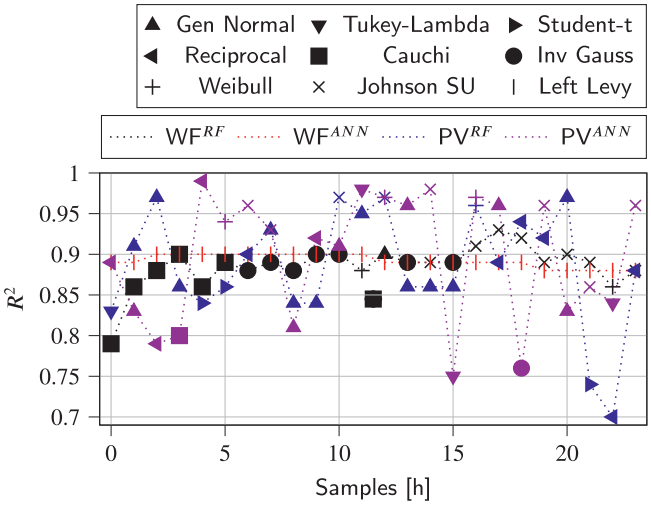

Fig. 4. Error distribution per method and resource.

efficiency. Lastly, the scheduled DA electrical and water demand are presented in Fig. 5; while hourly prices are presented in Fig. 6 based on typical days of the Iberian market during 2019 (to avoid COVID-related price disruptions). Note that the reserve requirements are assumed to be symmetric and 25% of the scheduled production which is paid at 10% of the DA rate. There is a penalty of 300 €/MWh for unserved energy, and water price is assumed at a flat rate, however, the associated production cost vary along with the HyPP operation.

4.1. Study case A: forecaster influence

The RES resource of 2 representative days are presented in Fig. 7, along with the confidence interval obtained from the predictors using 5 quantile bins. The results are presented in Table 1. The optimization performance is best when implementing the CNN-LSTM predictor despite its slightly lower accuracy. This is not particularly surprising as lower accuracy predictors have already been reported as better candidates for optimization systems in [52]. The solving time is quite fast for all scenarios and their differences of about 1 second are negligible as this optimization is run for 24 hours ahead. Given the higher RES availability of the winter day it is expected to present higher curtailment. An observed limitation is the final SOC of the water deposit. Since it reaches 100% a simulation with a longer horizon will not be able to exploit its flexibility unless it is followed by low RES availability periods. However, since the proposed dispatcher can be round at higher sampling rates, for instance once every few minutes, it would be possible to adapt the plant's operation live.

Fig. 8 presents the operational DA setpoints of the different units during each day using the CNN-LSTM forecaster; RF is omitted to avoid over-repetition and RT values due to the large number of scenarios. Briefly, during summer day the WS SOC is increased progressively until hour 7 then discharged until hour 12 and then filled up to 100% by the

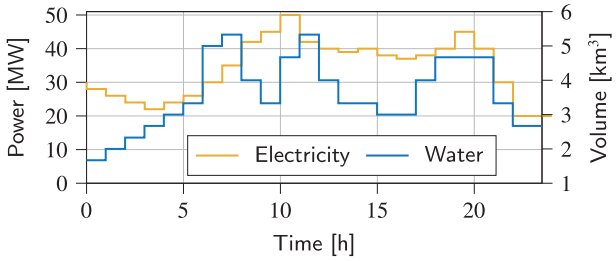

Fig. 5. Scheduled DA production.

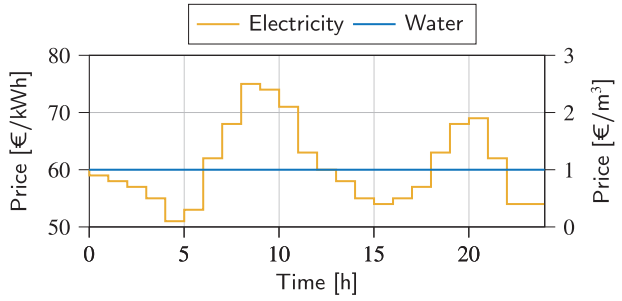

Fig. 6. Electricity and water prices.

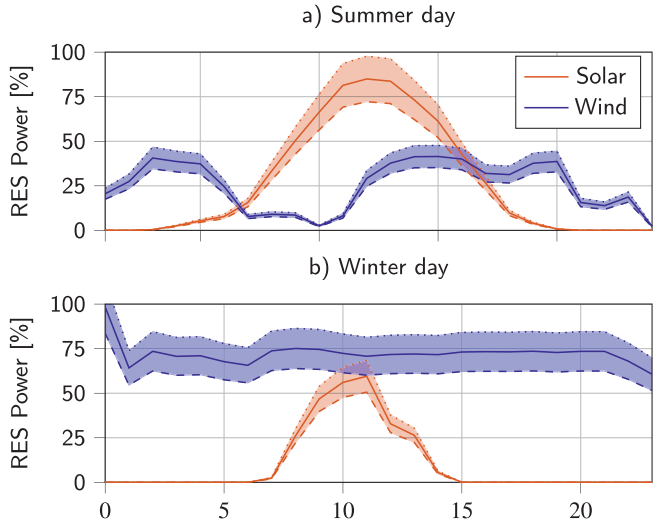

Fig. 7. Solar and wind resources.

Table 1
Results of Study Case A.

Day	A	B	A	B
Forecasters	RF	RF	CNN-LSTM	CNN-LSTM
Time [s]	6.4	6.7	6.3	7.1
Objective [€]	23.5	26.8	23.6	27.1
WS level [%]	100	100	100	100
Curtailment [%]	7.6	15	7.3	20

end of the day. Regarding the DA scheduling of desalination, MSF takes constant mid-low values slowly ramping up and down, while RO stays in a support role; only turning on when the ramping capabilities of the MSF are not sufficient. In this sense, MSF satisfies the bulk water demand, while RO adjusts matches the production. This operational synergies result particularly useful to accommodate renewables; presenting between 3 and 4% curtailment by the end of the optimization. Furthermore, the SMR maintains nominal output power during the whole day, simply adjusting its electric and heat ratios trying to match the remaining electrical production based on the available RES. On the other hand, in the winter scenario, the WS fills up slowly and continuously during the whole simulation solely fed by the MSF; which is able to accommodate all production and provide all the necessary rampings. This is due to the higher RES availability, since in this scenario a bigger fraction of the reactor's heat can be supplied to the desalination. Nevertheless, the curtailment also increases during this scenario ranging from 8 to 10% affecting mostly the WF.

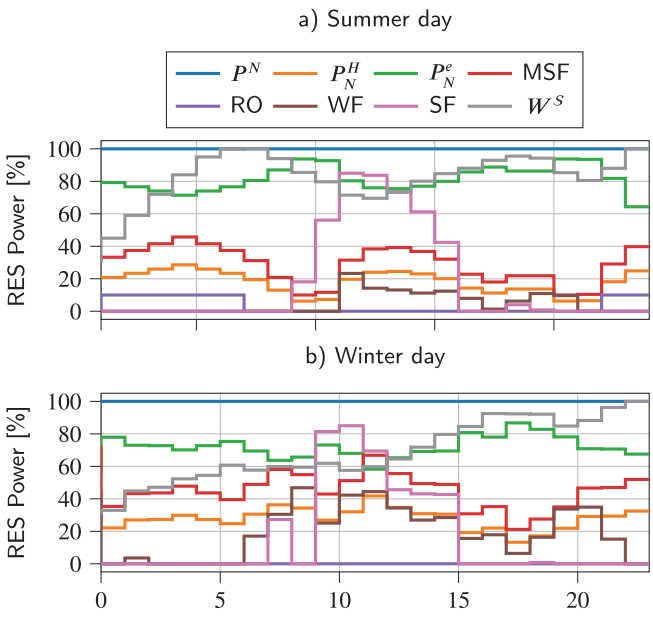

Fig. 8. Study Case A: Operational Summary.

4.2. Study case B: quantile number influence

In this study case the winter day is recalculated using 3, 5, 10, 50, and 100 quantile uncertainty bins for the RF forecaster. The number of scenarios grows quadratically with increasing bins, hence the solving speed is expected to deteriorate relatively fast. Clearly, the optimization exactness also increases with the number of considered scenarios, however the actual result does not necessary have to improve. Hence, an uncertainty free scenario is included as a deterministic (Det) case to assess what would be the systems behaviour with perfect information.

The results of this study case are presented in Table 2. There it can be seen how the cases with lower number of bins get an objective closer to the deterministic. Regarding curtailment, this is reduced along with the increasing number of bins as the error distribution is better captured; while the solving time grows with an opposite relation. A practical implementation should carefully asses the number of bins to be included based on the obtained accuracy and additional computational time required. In principle, the proposed formulation can be easily adapted to higher sampling rates in the minute scale, however, that will limit the bin number significantly and might not be translated into additional revenue.

4.3. Discussion

In general, the EMS has proven to effectively coordinate all the different generation and demand responsive units in order to satisfy the required demand and the different operational constraints. It is clear how the different temporal inertias of the different desalination technologies are exploited to accommodate higher rates of renewables and limit the effect on the core's reaction. Study Case A focused on the forecaster accuracy influence over the EMS performance while B

Table 2
Results of Study Case B.

Bin #	3	5	10	50	100	Det
Day	A	A	A	A	A	A
Forecasters	RF	RF	RF	RF	RF	–
Time [s]	3.9	6.4	23.1	112.7	896.5	0.9
Objective [€]	23.4	23.5	21.2	21.9	22.0	26.8
WS level [%]	100	100	84	100	100	100
Curtailment [%]	14.4	7.6	7.1	6.7	5.3	0

explored the influence of the uncertainty characterisation over the optimization results.

Since this is a purely theoretical study it is tough to validate the quantitative impact this approach could have on a real system. However, we can provide an estimation considering the case of a typical warm island such as Santiago, Cape Verde. There, desalination is the most energy intensive process which requires about a third of the overall electricity production and its associated emissions (50 kt of CO2 in 2019). With a peak load of around 40 MW, Santiago cover its energy needs with a 99 MW of fossil fueled generators, 9 MW of WF and 4.4 MW of SF, however its RES-rates have been limited below 20% due to stability concerns. Therefore a HyPP such as the proposed in this work will contribute both in terms of inertia, RES, and decarbonization; being able to power the whole island assuming enough transmission capacity. Overall, the proposed configuration could save between 46 and 59 tons of CO2 annually. The commissioning, and construction of such a HyPP present of course a number of challenges specially for a developing country, however those concerns fall beyond the scope of this work. [53,54]

5. Conclusion

The scientific community has the duty to address the incoming water crisis and ongoing energy transition simultaneously. Aiming to facilitate carbon-free and freshwater production for any global region; this paper proposed a coordination strategy for a HyPP in the form of an EMS formulated as an optimal SUC. The HyPP concept combines an SMR, WF, PV plant, two different desalination plants (RO and MSF) and freshwater storage. The dispatcher coordinates the SMR's core reaction, heat, water and electric systems to satisfy hourly water and electricity demand. In this sense, the EMS benefits the full power operation of the SMR in order to increase its lifetime and reliability, which causes renewables and sector coupling to provide the necessary flexibility.

The EMS assumes a MILP stochastic formulation to address RES uncertainty, hence requiring forecasts and scenario modeling. The former is address using ML, while the later are characterised by fitting the forecast's residual to statistical distribution following an unsupervised approach. The proposed EMS is evaluated with two different study cases. The first focused on validating the flexibility enabling capacity using different reference days. While the second focuses on exploring the computational performance and accuracy of the scenario characterisation method by varying the complexity of the residual fitting strategy. The results show how the proposed EMS effectively achieves a high degree of renewable integration, minimizing curtailment, by fully exploiting the synergies between electricity, heat, and water sectors, while smoothly operating the SMR.

Based on the presented results, the dispatcher appears suitable for larger resolution than 1 hour. However, the specific number of scenarios must be addressed to ensure achieving a satisfactory threshold between computational complexity and solving time. Future work will involve the implementation of the proposed formulation in a real microgrid environment.

Complementary data

The interested reader can access the full description of the implemented parameters for each unit, renewable resource curves, demand and price profiles in https://doi.org/10.11583/DTU.19222434.v1 [56]. Note to reviewers, the link will be updated to a DOI upon acceptance, the url is a private link for review purposes only.

CRediT authorship contribution statement

Daniel Vázquez Pombo: Conceptualization, Methodology, Software, Validation, Formal analysis, Data curation, Writing – original draft, Visualization, Writing – review & editing. **Henrik W. Bindner:** Resources, Supervision. **Sergiu V. Spataru:** Resources, Supervision. **Poul E. Sørensen:** Supervision, Project administration. **Martin Rygaard:** Conceptualization, Writing – original draft.

Declaration of competing interest

The authors declare that they have no known competing financial interests or personal relationships that could have appeared to influence the work reported in this paper. The authors declare no conflicts of interest.

Annex A. EMS Mathematical Formulation

The problem is conceptualised as a MILP stochastic formulation coordinating the different subplants conforming the HyPP as an optimal dispatcher to maximize its profits. DA market prices are given, and RES-related uncertainty is integrated using scenarios. The objective function defined in (5) is expressed as the minimization of the costs ($\mathscr{C}$) minus the income ($\mathscr{I}$). The costs are related to operation (a), start-up (b), shut-down (c), and deviation from nominal power of the fission reaction (d); as covered in (6)–(12).

$$\min_{\Xi} \quad \sum_{t}^{T} \mathscr{C}_t^a + \mathscr{C}_t^b + \mathscr{C}_t^c + \mathscr{C}_t^d + \mathscr{C}_t^f - \mathscr{I}_t^e - \mathscr{I}_t^w, \forall t \in T \tag{5}$$

$$\mathscr{C}_t^a = \sum_{g}^{\mathscr{G}} \left(P_{t,g}^e \rho_{t,g}^a + R_{t,g}^U \rho_{t,g}^U + R_{t,g}^D \rho_{t,g}^D \right) + \sum_{d}^{\mathscr{D}} \left(P_{t,d}^e \rho_{t,d}^a + R_{t,d}^U \rho_{t,d}^U + R_{t,d}^D \rho_{t,d}^D \right) + \sum_{\phi}^{\Phi} \chi_\phi \left[\rho_{t,g}^a \left(r_{t,\phi,g}^U - r_{t,\phi,g}^D \right) + \rho_{t,d}^a \left(r_{t,\phi,d}^D - r_{t,\phi,d}^U \right) + \sum_{r}^{\mathscr{G}^R} \rho_{t,r}^c P_{t,\phi,r}^c \right], \quad \forall t \tag{6}$$

$$\mathscr{C}_t^b \geq \sum_{j}^{\mathscr{J}} \rho^b \left(\nu_{t,j} - \nu_{t-1,j} \right), \ \forall t \neq 0, \forall j \in \mathscr{G} \cup \mathscr{D} \tag{7}$$

$$\mathscr{C}_t^c \geq \sum_{j}^{\mathscr{J}} \rho^c \left(\nu_{t-1,j} - \nu_{t,j} \right), \quad \forall t \neq 0 \forall j \in \mathscr{G} \cup \mathscr{D} \tag{8}$$

$$\mathscr{C}_t^d \geq \sum_{n}^{\mathscr{G}^N} \rho^d \left(P_{t,n} - P_{t-1,n} \right), \quad \forall t < \overline{T} \forall n \in \mathscr{G}^N \tag{9}$$

$$\mathscr{C}_t^d \geq \sum_{n}^{\mathscr{G}^N} \rho^d \left(P_{t-1,n} - P_{t,n} \right), \quad \forall t < \overline{T} \forall n \in \mathscr{G}^N \tag{10}$$

$$\mathscr{C}_t^f \geq \sum_n^{\mathscr{G}^N} \rho_n^f \left(\overline{H}_n - P_{t,n}^N\right), \quad \forall t \forall n \in \mathscr{G}^N \tag{11}$$

$$\mathscr{C}_{t,j}^b, \mathscr{C}_{t,j}^c, \mathscr{C}_t^d, \mathscr{C}_t^f \geq 0, \quad \forall t, \forall j \in \mathscr{G} \cup \mathscr{D} \tag{12}$$

The HyPP's income is related to selling electricity (e) and freshwater (w) as per eqs. (13)–(14). Alternatively, systems without water storage (WS) reformulate (14) as (15).

$$\mathscr{I}_t^e = \sigma_t^{e,d}\left[\sum_g^{\mathscr{G}} P_{t,g}^e + \sum_\phi^{\Phi} \chi_\phi \left(r_{t,\phi,g}^U - r_{t,\phi,g}^D\right) - \sum_d^{\mathscr{D}} P_{t,d}^e - \sum_\phi^{\Phi} \chi_\phi \left(r_{t,\phi,d}^U - r_{t,\phi,d}^D\right)\right] + \sigma_t^{e,U}\left(\sum_g^{\mathscr{G}} R_{t,g}^U + \sum_d^{\mathscr{D}} R_{t,d}^D\right) + \sigma_t^{e,D}\left(\sum_g^{\mathscr{G}} R_{t,g}^D + \sum_d^{\mathscr{D}} R_{t,d}^U\right), \ \forall t, \tag{13}$$

$$\mathscr{I}_t^w = \sigma_t^w W_t^{ds}, \quad \forall t, \tag{14}$$

$$\mathscr{I}_t^w = \sigma_t^w \sum_d^{\mathscr{D}} \left[P_{t,d}^e + \sum_\phi^{\Phi} \chi_\phi \left(r_{t,\phi,d}^D - r_{t,\phi,d}^U\right)\right] \eta_{t,d}, \quad \forall t, \tag{15}$$

Upper and lower operational bounds are defined in (16)–(17), which are then coupled to the reserves with (18)–(21).

$$0 \leq P_{t,j}^a \leq Q_{t,j}, \quad \forall t, \forall j \in \mathscr{G} \cup \mathscr{D} \tag{16}$$

$$\underline{P_j} \nu_{t,j} \leq P_{t,j}^a, \quad \forall t, \forall j \in \mathscr{G} \cup \mathscr{D} \tag{17}$$

$$P_{t,g}^a + R_{t,g}^U \leq Q_{t,g}, \quad \forall t, \forall g \in \mathscr{G} \tag{18}$$

$$P_{t,g}^a - R_{t,g}^D \geq 0, \quad \forall t, \forall g \in \mathscr{G} \tag{19}$$

$$P_{t,d}^a + R_{t,d}^D \leq Q_{t,d}, \quad \forall t, \forall d \in \mathscr{D} \tag{20}$$

$$P_{t,d}^a - R_{t,d}^U \geq 0, \quad \forall t, \forall d \in \mathscr{D} \tag{21}$$

The maximum possible production (Q) is coupled to the on/off state with (22)–(23). This state is defined with a binary variable ν (24), where 1 corresponds to the on state and vice versa.

$$0 \leq Q_{t,j} \leq \overline{P_j} \nu_{t,j}, \quad \forall t, \forall j \in \mathscr{G} \cup \mathscr{D} \tag{22}$$

$$Q_{t,r} \leq \overline{P_r} \nu_{t,r} \widetilde{P_{t,r}}, \quad \forall t, \forall r \in \mathscr{G}^R \tag{23}$$

$$\nu_{t,j}, \in \{0,1\}, \quad \forall t, \forall j \in \mathscr{G} \cup \mathscr{D} \tag{24}$$

Dynamics related to upward and downward rampings, startup and stopping limits are defined with (25)–(27).

$$Q_{t,j} \leq P_{t-1,j}^a + \overline{U_j^R} \nu_{t-1,j} + \overline{U_j^s}\left(\nu_{t,j} - \nu_{t-1,j}\right) + \overline{P_j}\left(1 - \nu_{t,j}\right), \quad \forall t > 1, \forall j \in \mathscr{G} \cup \mathscr{D} \tag{25}$$

$$Q_{t,j} \leq \overline{P_j} \nu_{t+1,j} + \overline{D_j^s}\left(\nu_{t,j} - \nu_{t+1,j}\right), \forall t < T, \forall j \in \mathscr{G} \cup \mathscr{D} \tag{26}$$

$$P_{t-1,j}^a - P_{t,j}^a \leq \overline{D_j^R} \nu_{t,j} + \overline{D_j^s}\left(\nu_{t-1,j} - \nu_{t,j}\right) + \overline{P_j}\left(1 - \nu_{t-1,j}\right), \forall t > 1, \forall j \in \mathscr{G} \cup \mathscr{D} \tag{27}$$

Limits related to on and off periods are defined in (28)–(30), and (31)–(33), respectively.

$$\sum_{\mathrm{k}=1}^{\overline{T0_j^{up}}} \left(1 - \nu_{k,j}\right) = 0, \quad \forall j \in \mathscr{G} \cup \mathscr{D} \tag{28}$$

$$\sum_{n=k}^{k+\underline{T_j^{up}}-1} \nu_{n,j} \geq \underline{T_j^{up}}\left(\nu_{k,j} - \nu_{k-1,j}\right), \forall j \in \mathscr{G} \cup \mathscr{S} \cup \mathscr{D}, \forall k = \underline{T0_j^{up}} + 1 \ldots T - \underline{T_j^{up}} + 1 \tag{29}$$

$$\sum_{n=k}^{T} \left(\nu_{n,j} - \left(\nu_{k,j} - \nu_{k-1,j}\right)\right) \geq 0, \forall j \in \mathscr{G} \cup \mathscr{S} \cup \mathscr{D}, \forall k = T - \underline{T_j^{up}} + 2 \ldots T \tag{30}$$

$$\sum_{\mathrm{k}=1}^{\overline{T0_j^{down}}} \nu_{k,j} = 0, \quad \forall j \in \mathscr{G} \cup \mathscr{S} \cup \mathscr{D} \tag{31}$$

$$\sum_{\mathrm{n}=k}^{k+\underline{T_j^{down}}-1} \left(1 - \nu_{n,j}\right) \geq \underline{T_j^{down}}\left(\nu_{k-1,j} - \nu_{k,j}\right), \forall j \in \mathscr{G} \cup \mathscr{S} \cup \mathscr{D}, \forall k = \underline{T0_j^{down}} + 1 \ldots T - \underline{T_j^{down}} + 1 \tag{32}$$

$$\sum_{n=k}^{T} \left(1 - \nu_{n,j} - \left(\nu_{k-1,j} - \nu_{k,j}\right)\right) \geq 0, \forall j \in \mathscr{G} \cup \mathscr{S} \cup \mathscr{D}, \forall k = T - \underline{T_j^{down}} + 2 \ldots T \tag{33}$$

Power balance, in DA and RT operations are established with (34)–(35).

$$\sum_{j}^{\mathscr{G}} P_{t,g}^{a} - \sum_{d}^{\mathscr{D}} P_{t,d}^{a} - \mathscr{L}_{t}^{e} = 0, \quad \forall t \tag{34}$$

$$\sum_{n}^{\mathscr{G}^N}\left(r_{t,\phi,n}^{U} - r_{t,\phi,n}^{D}\right) + \sum_{r}^{\mathscr{G}^R}\left(\mathscr{F}_{t,\phi,r} - P_{t,r}^{a} - r_{t,\phi,r}^{U} + r_{t,\phi,r}^{D} - P_{t,\phi,r}^{c}\right) + \sum_{d}^{\mathscr{D}}\left(r_{t,\phi,a}^{D} - r_{t,\phi,a}^{U}\right) = 0, \forall t \tag{35}$$

The overloading of the PCC is prevented by limiting the power exchanged as established with (36). While RT reserves are bounded by the scheduled bid with (37)–(38).

$$\sum_{g}^{\mathscr{G}}\left(P_{t,g}^{a} + R_{t,g}^{U}\right) - \sum_{d}^{\mathscr{D}}\left(P_{t,d}^{a} - R_{t,d}^{U}\right) - \mathscr{L}_{t}^{e} \leq \overline{PCC}, \tag{36}$$

$$r_{t,\phi,j}^{U} \leq R_{t,j}^{U}, \quad \forall t, \forall j \in \mathscr{G} \cup \mathscr{D} \tag{37}$$

$$r_{t,\phi,j}^{D} \leq R_{t,j}^{D}, \quad \forall t, \forall j \in \mathscr{G} \cup \mathscr{D} \tag{38}$$

SMR operation is defined by eqs. (39)–(41), which bound the operation of the reactor, electrical production, and excess heat, respectively. To avoid wasting the excess heat, constraint (42) couples it with the heat demanded by water desalination units ($\mathscr{E}$). Then, the electrical power necessary for completing the desalination process is set with eq. (43).

$$0 \leq P_{t,n}^{N} \leq \overline{H}_{n}, \quad \forall t, \forall n \in \mathscr{G}^{N} \tag{39}$$

$$0 \leq P_{t,n}^{H} \leq P_{t,n}^{N}, \quad \forall t, \forall n \in \mathscr{G}^{N} \tag{40}$$

$$P_{t,n}^{N} = P_{t,n}^{H} + P_{t,n}^{a}\overline{H}_{n}\Big/\overline{P}_{n}, \quad \forall t, \forall n \in \mathscr{G}^{N} \tag{41}$$

$$P_{t,n}^{H} = P_{t,e}^{H}, \quad \forall t, \forall n \in \mathscr{G}^{N}, \forall e \in \mathscr{E} \tag{42}$$

$$P_{t,e}^{H} = P_{t,e}^{a}\gamma_{e}, \quad \forall t, \forall e \in \mathscr{E} \tag{43}$$

Water requirements can be set by establishing a set of lower and upper bounds for its daily production using eq. (44). However, if a demand curve must be served, water balance is expressed as (45)–(46) or (47)–(48) depending on the WS inclusion.

$$\underline{E}^{T} \leq \sum_{t}^{t+T}\gamma_{d}P_{t,d}^{a} \leq \overline{E}^{T}, \quad \forall t, \forall d \in \mathscr{D} \tag{44}$$

$$W_{t}^{ch} = \sum_{d}^{\mathscr{D}}\left[P_{t,d}^{a} + \sum_{\phi}^{\Phi}\chi_{\phi}\left(r_{t,\phi,d}^{D} - r_{t,\phi,d}^{U}\right)\right]\eta_{t,d}, \forall t \tag{45}$$

$$W_{t}^{ds} - \mathscr{D}_{t}^{w} = 0, \quad \forall t \tag{46}$$

$$\mathscr{D}_{t}^{w} = \sum_{d}^{\mathscr{D}} P_{t,d}^{a}\eta_{t,d} \tag{47}$$

$$\mathscr{D}_{t}^{w} = \sum_{d}^{\mathscr{D}}\left[P_{t,d}^{a} + \sum_{\phi}^{\Phi}\chi_{\phi}\left(r_{t,\phi,d}^{D} - r_{t,\phi,d}^{U}\right)\right]\eta_{t,d} \tag{48}$$

The WS discharging and charging dynamics are covered by (49)–(50), note that unlike other types of storage, WS can charge and discharge simultaneously due to piping redundancy. The stored volume is monitored with (51), whose minimum and maximum limits are established with (52), while its initial and final states are constrained with (53)–(54). These initial and final constraints are added to prevent depletion by the end of the horizon, and it is common practice for any type of storage.

$$0 \leq W_{t}^{ds} \leq \overline{W^{ds}} \tag{49}$$

$$0 \leq W_{t}^{ch} \leq \sum_{d}^{\mathscr{D}}\overline{P^{e}}_{d}\overline{\eta}_{d} \tag{50}$$

$$W_{t}^{\mathscr{S}} = W_{t-1}^{\mathscr{S}} + W_{t}^{ch} - W_{t}^{ds} \tag{51}$$

$$\underline{W}^{\mathscr{S}} \leq W_{t}^{\mathscr{S}} \leq \overline{W}^{\mathscr{S}} \tag{52}$$

$$W_{t}^{\mathscr{S}} = W^{\mathscr{S}_0}, \quad \forall t = 0, \tag{53}$$

$$W_{t}^{\mathscr{S}} \geq W^{\mathscr{S}_0}, \quad \forall t = T, \tag{54}$$

The cost function of nuclear generators (ρ^{a}) and efficiency curves of desalination plants (η) are conceptually represented in Fig. 9. These are

quadratic expressions of the form (55), that can be approximated with a set of a linear piecewise blocks, whose analytic formulation is covered in (56)–(60); where Y and y stand for the variable and its corresponding linearized value. The reader is recommended to check the work by Carrion et al. [55], which further elaborate this formulation.

$$Y_{t,j} = \alpha_j \nu_{t,j} + \beta_j P_{t,j} + \theta_j P_{t,j}^2, \quad \forall t, \forall j \tag{55}$$

$$Y_{t,j} = A_j^y \nu_{t,j} + \sum_l^L \pi_{l,j} \delta_{t,j}^l, \quad \forall t, \forall j \tag{56}$$

$$Y_{t,j} = \sum_l^L \delta_{t,j}^l + \underline{y}_j \nu_{t,j}, \quad \forall t, \forall j \tag{57}$$

$$0 \le \delta_{t,j}^l \le T_{l,j} - \overline{\underline{y}}_j, \quad \forall l = 1, \forall t, j \tag{58}$$

$$0 \le \delta_{t,j}^l \le T_{l,j} - T_{l-1,j} \overline{\underline{y}}_j, \forall l = 2 \cdots L_j - 1, \forall t, j \tag{59}$$

$$0 \le \delta_{t,j}^l \le \overline{\underline{y}}_j - T_{L-1,j}, \quad \forall l = L_j, \forall t, j \tag{60}$$

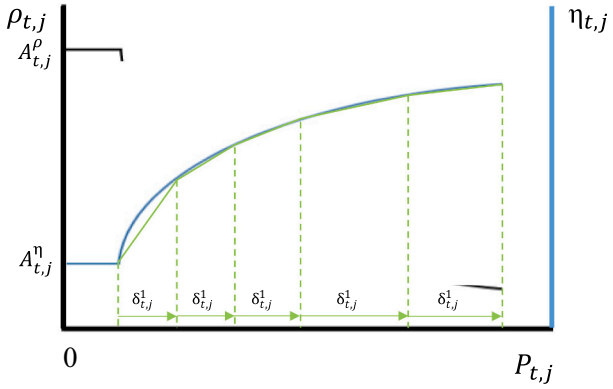

Fig. 9. Piecewise linear cost and efficiency representation.

References

[1] UNDESA, UNECE, UNECLAC, UNESCAP, Water for a sustainable world, in: World Water Development, 2015.

[2] M. Rygaard, P.J. Binning, H.-J. Albrechtsen, Increasing urban water self-sufficiency: new era, new challenges, J. Environ. Manag. 92 (1) (2011) 185–194.

[3] E.J. Okampo, N. Nwulu, Optimisation of renewable energy powered reverse osmosis desalination systems: a state-of-the-art review, Renew. Sust. Energ. Rev. 140 (2021), 110712.

[4] S. Tian, L. Guo, Y. Gu, S. Ju, L. Xu, Energy transfer and efficiency analysis of microwave flash evaporation with tap water as medium, Desalination 511 (2021), 115095.

[5] Z. Zhang, A. Atia, J. Andrés-Mañas, G. Zaragoza, V. Fthenakis, Comparative techno-economic assessment of osmotically-assisted reverse osmosis and batch-operated vacuum-air-gap membrane distillation for high-salinity water desalination, Desalination 532 (2022), 115737.

[6] N.A. Moharram, S. Bayoumi, A.A. Hanafy, W.M. El-Maghlany, Hybrid desalination and power generation plant utilizing multi-stage flash and reverse osmosis driven by parabolic trough collectors, Case Stud. Therm. Eng. 23 (2021), 100807.

[7] Z. Mo, C.D. Peters, C. Long, N.P. Hankins, Q. She, How split-feed osmotically assisted reverse osmosis (sf-oaro) can outperform conventional reverse osmosis (cro) processes under constant and varying electricity tariffs, Desalination 530 (2022), 115670.

[8] M.T. Mito, X. Ma, H. Albuflasa, P.A. Davies, Variable operation of a renewable energy-driven reverse osmosis system using model predictive control and variable recovery: towards large-scale implementation, Desalination 532 (2022), 115715.

[9] O. Lindberg, J. Arnqvist, J. Munkhammar, D. Lingfors, Review on power-production modeling of hybrid wind and pv power parks, J. Renew. Sustain. Energy 13 (4) (2021), 042702.

[10] K. Sadeghi, S.H. Ghazaie, R. Chebac, E. Sokolova, E. Fedorovich, A. Cammi, M. E. Ricotti, A.S. Shirani, Towards net-zero emissions through the hybrid smr-solar cogeneration plant equipped with modular pcm storage system for seawater desalination, Desalination 524 (2022), 115476.

[11] B. Liu, B. Zhou, D. Yang, G. Li, J. Cao, S. Bu, T. Littler, Optimal planning of hybrid renewable energy system considering virtual energy storage of desalination plant based on mixed-integer nsga-iii, Desalination 521 (2022), 115382.

[12] Y. Fang, S. Zhao, Z. Chen, Multi-objective unit commitment of jointly concentrating solar power plant and wind farm for providing peak-shaving considering operational risk, Int. J. Electr. Power Energy Syst. 137 (2022), 107754.

[13] Y. Yang, J.C.-H. Peng, C. Ye, Z.-S. Ye, Y. Ding, A criterion and stochastic unit commitment towards frequency resilience of power systems, IEEE Trans. Power Syst. 37 (1) (2021) 640–652.

[14] L. Le, J. Fang, M. Zhang, K. Zeng, X. Ai, Q. Wu, J. Wen, Data-driven stochastic unit commitment considering commercial air conditioning aggregators to provide multi-function demand response, Int. J. Electr. Power Energy Syst. 129 (2021), 106790.

[15] D. Van der Meer, G.C. Wang, J. Munkhammar, An alternative optimal strategy for stochastic model predictive control of a residential battery energy management system with solar photovoltaic, Appl. Energy 283 (2021), 116289.

[16] L. Amabile, D. Bresch-Pietri, G. El Hajje, S. Labbé, N. Petit, Optimizing the self-consumption of residential photovoltaic energy and quantification of the impact of production forecast uncertainties, Adv. Appl. Energy 2 (2021), 100020.

[17] T. Ahmad, H. Chen, A review on machine learning forecasting growth trends and their real-time applications in different energy systems, Sustain. Cities Soc. 54 (2020), 102010.

[18] R. Yuan, B. Wang, Z. Mao, J. Watada, Multi-objective wind power scenario forecasting based on pg-gan, Energy 226 (2021), 120379.

[19] M. Izadi, et al., A critical review on definitions, indices, and uncertainty characterization in resiliency-oriented operation of power systems, Int. Trans. Electr. Energy Syst. 31 (1) (2021), e12680.

[20] Y. Wen, D. AlHakeem, P. Mandal, S. Chakraborty, Y.-K. Wu, T. Senjyu, S. Paudyal, T.-L. Tseng, Performance evaluation of probabilistic methods based on bootstrap and quantile regression to quantify pv power point forecast uncertainty, IEEE Trans. Neural Netw. Learn. Syst. 31 (4) (2019) 1134–1144.

[21] H. Subki, Advances in Small Modular Reactor Technology Developments, International Atomic Energy Agency (IAEA), 2020.

[22] S.E. Arda, K.E. Holbert, Nonlinear dynamic modeling and simulation of a passively cooled small modular reactor, Prog. Nucl. Energy 91 (2016) 116–131.

[23] G. Locatelli, S. Boarin, F. Pellegrino, M.E. Ricotti, Load following with small modular reactors (smr): a real options analysis, Energy 80 (2015) 41–54.

[24] G. Locatelli, S. Boarin, A. Fiordaliso, M.E. Ricotti, Load following of small modular reactors (smr) by cogeneration of hydrogen: a techno-economic analysis, Energy 148 (2018) 494–505.

[25] G. Locatelli, A. Fiordaliso, S. Boarin, M.E. Ricotti, Cogeneration: an option to facilitate load following in small modular reactors, Prog. Nucl. Energy 97 (2017) 153–161.
[26] D. Ingersoll, Z. Houghton, R. Bromm, C. Desportes, Nuscale small modular reactor for co-generation of electricity and water, Desalination 340 (2014) 84–93.
[27] M. Qasim, M. Badrelzaman, N.N. Darwish, N.A. Darwish, N. Hilal, Reverse osmosis desalination: a state-of-the-art review, Desalination 459 (2019) 59–104.
[28] H. Nassrullah, S.F. Anis, R. Hashaikeh, N. Hilal, Energy for desalination: a state-of-the-art review, Desalination 491 (2020), 114569.
[29] K.C. Ng, K. Thu, S.J. Oh, L. Ang, M.W. Shahzad, A.B. Ismail, Recent developments in thermally-driven seawater desalination: energy efficiency improvement by hybridization of the med and ad cycles, Desalination 356 (2015) 255–270.
[30] H. Al-Fulaij, A. Cipollina, H. Ettouney, D. Bogle, Simulation of stability and dynamics of multistage flash desalination, Desalination 281 (2011) 404–412.
[31] O.A. Hamed, Overview of hybrid desalination systems—current status and future prospects, Desalination 186 (1–3) (2005) 207–214.
[32] F.E. Ahmed, R. Hashaikeh, N. Hilal, Hybrid technologies: the future of energy efficient desalination–a review, Desalination 495 (2020), 114659.
[33] J. Martinez-Rico, E. Zulueta, I.R. de Argandoña, U. Fernandez-Gamiz, M. Armendia, Multi-objective optimization of production scheduling using particle swarm optimization algorithm for hybrid renewable power plants with battery energy storage system, J. Mod. Power Syst. Clean Energy 9 (2) (2020) 285–294.
[34] M. Gökçek, Integration of hybrid power (wind-photovoltaic-diesel-battery) and seawater reverse osmosis systems for small-scale desalination applications, Desalination 435 (2018) 210–220.
[35] G.E. Karniadakis, I.G. Kevrekidis, L. Lu, P. Perdikaris, S. Wang, L. Yang, Physics-informed machine learning, Nat. Rev. Phys. 3 (6) (2021) 422–440.
[36] Daniel Vazquez Pombo, The SOLETE dataset. https://doi.org/10.11583/DTU.17040767, 2022, Feb. Retrieved from, https://data.dtu.dk/articles/dataset/The_SOLETE_dataset/17040767.
[37] D.V. Pombo, H.W. Bindner, S.V. Spataru, P.E. Sørensen, P. Bacher, Increasing the accuracy of hourly multi-output solar power forecast with physics-informed machine learning, Sensors 22 (3) (2022) 749.
[38] D.L. King, J.A. Kratochvil, W.E. Boyson, Photovoltaic Array Performance Model, United States. Department of Energy, 2004.
[39] D.V. Pombo, T. Göçmen, K. Das, P. Sørensen, Multi-horizon data-driven wind power forecast: from nowcast to 2 days-ahead, in: 2021 International Conference on Smart Energy Systems and Technologies (SEST), IEEE, 2021, pp. 1–6.
[40] M. Bozorg, A. Bracale, P. Caramia, G. Carpinelli, M. Carpita, P. De Falco, Bayesian bootstrap quantile regression for probabilistic photovoltaic power forecasting, Prot. Control Mod. Power Syst. 5 (1) (2020) 1–12.
[41] B.-M. Hodge, M. Milligan, Wind power forecasting error distributions over multiple timescales, in: 2011 IEEE Power and Energy Society General Meeting, IEEE, 2011, pp. 1–8.
[42] J. Wu, B. Zhang, H. Li, Z. Li, Y. Chen, X. Miao, Statistical distribution for wind power forecast error and its application to determine optimal size of energy storage system, Int. J. Electr. Power Energy Syst. 55 (2014) 100–107.
[43] P. Yan, C. Xiang, T. Li, X. Hu, W. Zhou, L. Wang, L. Meng, Research on probability distribution of short-term photovoltaic output forecast error based on numerical characteristic clustering, Comput. Intell. Neurosci. 2022 (2022).
[44] P. Virtanen, et al., SciPy 1.0: fundamental algorithms for scientific computing in Python, Nat. Methods 17 (2020) 261–272.
[45] J. Lemos-Vinasco, P. Bacher, J.K. Møller, Probabilistic load forecasting considering temporal correlation: online models for the prediction of households' electrical load, Appl. Energy 303 (2021), 117594.
[46] S. Jerez, I. Tobin, M. Turco, P. Jiménez-Guerrero, R. Vautard, J. Montávez, Future changes, or lack thereof, in the temporal variability of the combined wind-plus-solar power production in Europe, Renew. Energy 139 (2019) 251–260.
[47] W.E. Hart, J.-P. Watson, D.L. Woodruff, Pyomo: modeling and solving mathematical programs in Python, Math. Program. Comput. 3 (3) (2011) 219–260.
[48] M. Al-Obaidi, G. Filippini, F. Manenti, I.M. Mujtaba, Cost evaluation and optimisation of hybrid multi effect distillation and reverse osmosis system for seawater desalination, Desalination 456 (2019) 136–149.
[49] G.A. Black, F. Aydogan, C.L. Koerner, Economic viability of light water small modular nuclear reactors: general methodology and vendor data, Renew. Sust. Energ. Rev. 103 (2019) 248–258.
[50] S. Bouckaert, A.F. Pales, C. McGlade, U. Remme, B. Wanner, "Net Zero by 2050 a Roadmap for the Global Energy Sector," Tech. Rep, International Energy Agency, May 2021.
[51] W. Cole, A.W. Frazier, C. Augustine, "Cost Projections for Utility-scale Battery Storage: 2021 Update," Tech. Rep, National Renewable Energy Lab.(NREL), Golden, CO (United States), 2021.
[52] L. Alvarado-Barrios, A.R. del Nozal, J.B. Valerino, I.G. Vera, J.L. Martínez-Ramos, Stochastic unit commitment in microgrids: influence of the load forecasting error and the availability of energy storage, Renew. Energy 146 (2020) 2060–2069.
[53] D.V. Pombo, H.W. Bindner, P. Sorensen, E. Fonseca, H. Andrade, The Islands of Cape Verde as a reference system for 100% renewable deployment, in: 2021 IEEE Green Technologies Conference (GreenTech), (Denver, CO, USA), IEEE, Apr. 2021, pp. 455–461.
[54] D.V. Pombo, Cape Verde Reference System v2.0, Retrieved from DTU-Data, https://data.dtu.dk/articles/dataset/Cape_Verde_Reference_System_v2_0/17430413, Feb 2022, https://doi.org/10.11583/DTU.17430413.v1.
[55] M. Carrión, J.M. Arroyo, A computationally efficient mixed-integer linear formulation for the thermal unit commitment problem, IEEE Trans. Power Syst. 21 (3) (2006) 1371–1378.
[56] Daniel Vazquez Pombo, Complementary data for Machine Learning-Driven Energy Management of a Hybrid Nuclear-Wind-Solar-Desalination Plant. https://doi.org/10.11583/DTU.19222434.v1, 2022, May. Retrieved from, https://data.dtu.dk/articles/dataset/Complementary_data_for_Machine_Learning-Driven_Energy_Management_of_a_Hybrid_Nuclear-Wind-Solar-Desalination_Plant/19222434.